Oxidation-State Control of Nanoparticles Synthesized via Chemical Reduction Using Potential Diagrams

Shunsuke Yagi,*,z Hidetaka Nakanishi, Tetsu Ichitsubo, and Eiichiro Matsubara

Department of Materials Science and Engineering, Kyoto University, Kyoto 606-8501, Japan

A general concept for oxidation-state control of nanoparticles synthesized via chemical reduction has been developed. By comparing kinetically determined mixed potential measured in reaction solution and thermodynamically drawn potential diagrams, e.g., potential–pH diagram, it is possible to know "what chemical species is stable in the reaction solution?." It is predicted from potential diagrams that nanoparticles in different oxidation states can be selectively synthesized by controlling mixed potential. This concept is verified by selectively synthesizing Cu and Cu_2O nanoparticles from CuO aqueous suspension via chemical reduction using the concept as an example. The dependency of mixed potential on pH and temperature is discussed in detail for the selective synthesis of nanoparticles.
© 2009 The Electrochemical Society. [DOI: 10.1149/1.3151966] All rights reserved.

Copper (Cu) nanoparticles are of great interest in various fields, specifically that of printable electronics. Cu interconnects less than 20 μm wide can be made with a high resolution screen printer or a super inkjet printer using an ink which contains dense Cu nanoparticles. Cu nanoparticles have been synthesized by various reduction processes from cupric or cuprous compounds, including direct electrochemical reduction,[1-3] chemical reduction,[4-8] thermal reduction,[9] sonochemical reduction,[9,10] laser irradiation,[11] and gamma radiolysis.[12] Many of these methods are conducted in liquid phase and are often called "liquid-phase reduction." Liquid-phase reduction can generate nanoparticles in large quantity in a single process and also has the important advantage that nanoparticles can be formed in the presence of dispersing agents and no additional process for the addition of dispersing agents is required for the fabrication of inks to avoid the agglomeration.

Cuprous oxide (Cu_2O) is a p-type semiconductor[13] and is also a promising material with potential applications in solar energy conversion, microelectronics, magnetic storage, catalysis, and gas sensing.[14] Cu_2O is also used for the investigation into Bose–Einstein condensation of excitons.[15] Many methods have been reported to synthesize Cu_2O nanoparticles,[14,16,17] nanocubes,[18,19] octahedral nanocages,[20] and nanowires.[21] For example, Muramatsu and Sugimoto reported that Cu_2O particles with an average diameter of 270 nm were synthesized in large quantities from a CuO aqueous suspension using hydrazine as the reducing agent.[16] Liu et al. formed CuO, Cu_2O, and Cu nanoparticles using copper(II) acetylacetonate $[Cu(acac)_2]$ as a precursor in oleylamine by controlling temperature.[17] Although many synthesis methods of Cu and Cu_2O nanoparticles have been reported, the synthesis processes have not been well discussed from the viewpoint of thermodynamics.

Against such a background, we propose a general concept for oxidation-state control of nanoparticles synthesized by chemical reduction using potential diagrams. In the present paper, the concept for oxidation-state control is described and verified by selectively synthesizing Cu and Cu_2O nanoparticles from a CuO aqueous suspension by chemical reduction as an example. The advantage of this chemical reduction method in liquid phase is that abundant nanoparticles can be obtained for a short time by a simple operation.[22,23] An extremely small activity of Cu^{2+} aquo ion is achieved by using insoluble CuO powder as a Cu(II) ionic source, which is a key for the synthesis of nanosized particles.

Theory

In this section, a general concept for selective synthesis of nanoparticles will be introduced. All the data considered and used for thermodynamic calculation are listed in Table I.[24-27] The constant *a*

and coefficients *b* and *c* for the specific-heat capacity of hydrazine are only estimated by fitting the discrete data of the specific heat capacity of hydrazine in the temperature range from 100 to 600 K.[27]

At any point within the reaction volume, several partial reactions occur in parallel. The potential at a point is determined at the value where the total of anodic currents $I_{a,total}$ balances the total of cathodic currents $I_{c,total}$ unless current flows outside (Fig. 1). This potential is called the mixed potential. Stable chemical species in the reaction solution can be determined by comparing measured mixed potential and calculated potential diagrams, and chemical species synthesized can be changed by controlling mixed potential.

As an example, considering a reaction system for the synthesis of Cu or Cu_2O nanoparticles from a CuO aqueous suspension of pH 9 via hydrazine reduction, anodic reactions are mainly the oxidation reactions of hydrazine as follows

$$N_2H_4 + 4OH^- \rightarrow N_2 + 4H_2O + 4e \quad [1]$$

$$N_2H_4 + OH^- \rightarrow \tfrac{1}{2}N_2 + NH_3 + H_2O + e \quad [2]$$

Cathodic reactions are mainly the reaction of the deposition of Cu or Cu_2O and hydrogen generation reaction as follows

Deposition of copper

$$Cu(II) + 2e \rightarrow Cu \quad [3]$$

Deposition of cuprous oxide

$$2Cu(II) + 2OH^- + 2e \rightarrow Cu_2O + H_2O \quad [4]$$

Hydrogen generation

$$2H_2O + 2e \rightarrow H_2 + 2OH^- \quad [5]$$
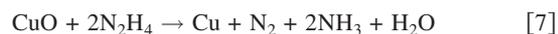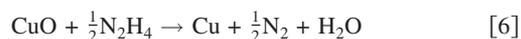
where Cu(II) represents all the copper(II) species and is distinguished from a copper(II) aquo ion, Cu^{2+}. The overall deposition reactions of Cu and Cu_2O in this system can be expressed using the following equations

Deposition of copper

$$CuO + \tfrac{1}{2}N_2H_4 \rightarrow Cu + \tfrac{1}{2}N_2 + H_2O \quad [6]$$

$$CuO + 2N_2H_4 \rightarrow Cu + N_2 + 2NH_3 + H_2O \quad [7]$$

Deposition of cuprous oxide

$$2CuO + \tfrac{1}{2}N_2H_4 \rightarrow Cu_2O + \tfrac{1}{2}N_2 + H_2O \quad [8]$$

$$2CuO + 2N_2H_4 \rightarrow Cu_2O + N_2 + 2NH_3 + H_2O \quad [9]$$

Figure 2 shows potential–pH diagrams (Pourbaix diagrams)[28] drawn at an equilibrium activity of the Cu^{2+} aquo ion in the presence of abundant CuO at pH 9. In this case, the equilibrium activity of Cu^{2+} aquo ion can be determined by considering an equilibrium reaction

* Electrochemical Society Active Member.
z E-mail: syagi@mtl.kyoto-u.ac.jp

Table I. List of standard heat of formation, entropy at 298 K and 1 atm, and specific heat at constant pressure (1 atm) considered and used for thermodynamic calculation.

Chemical species	Standard heat of formation (kJ mol^{-1})	Standard entropy (J K^{-1} mol^{-1})	Specific heat at constant pressure (J K^{-1} mol^{-1}) $C_p = a + b \times 10^{-3}\,T + c \times 10^5\,T^2$			References
			a	b	c	
H$^+$ (aq)	0.0	0.0	129.7	—	—	24 and 25
Cu^{2+} (aq)	64.4	−98.7	267.8	—	—	24 and 25
H$_2$O (l)	−285.8	70.0	75.4	—	—	26
H$_2$ (g)	0.0	130.6	27.3	3.3	0.50	26
Cu (s)	0.0	33.1	22.6	6.3	—	26
Cu$_2$O (s)	−167.4	93.1	62.3	23.9	—	26
CuO (s)	−155.2	42.7	38.8	20.1	—	26
N$_2$ (g)	0.0	191.5	27.9	4.3	—	26
NH$_3$ (g)	−45.9	192.7	37.3	18.7	−6.49	26
N$_2$H$_4$ (l)	50.6	121.6	72.7	87.2	0.60	27

of Cu^{2+} and CuO, where the activities of CuO and H$^+$ are assigned to 1 and 10^{-9}, respectively. The species Cu^{2+}, CuO, Cu$_2$O, and Cu are only considered, and oxyanions of copper, such as HCuO$_2^-$ and CuO$_2^{2-}$, or hydroxyanions of copper,[29] Cu(OH)$_3^-$ and Cu(OH)$_4^{2-}$, are not considered. This is only for simplicity because the oxidation–reduction potentials of CuO/Cu$_2$O and Cu$_2$O/Cu redox pairs at pH 9 are important for the prediction of synthesized chemical species in this case. For instance, the oxidation–reduction potentials of Cu$_2$O and any Cu(II) ionic species in equilibrium are the same at a constant pH and temperature in the presence of abundant solid CuO powder, resulting in the same oxidation–reduction potential of the Cu$_2$O/Cu redox pair. The equilibrium activity of Cu^{2+} aquo ion changes with pH and therefore, the potential–pH diagram is only valid at the constant pH considered. Fortunately, pH of the solution barely changes during the reaction in the present method,[22] and it is possible to determine the most stable chemical species throughout the reaction by comparing the measured mixed potential to the vertical line of a constant pH (in this case, pH 9) in the potential–pH diagrams. In other words, the kind of chemical species synthesized can be controlled if the mixed potential is changed as expected. Next, factors to change the mixed potential are discussed.

As described above, the mixed potential is determined by the balance of each partial current. Therefore, the mixed potential is changed when the oxidation–reduction potential of each partial reaction is changed. The oxidation–reduction potential E at a temperature T and 1 atm is calculated using the following Nernst equation

$$E = -\frac{\Delta G_T}{nF} = -\frac{1}{nF}(\Delta G_T^0 + RT \ln Q)$$

$$= -\frac{1}{nF}[(\Delta H_T^0 - T\Delta S_T^0) + RT \ln Q]$$

$$= -\frac{1}{nF}\left[\left(\Delta H_{298}^0 + \int_{298}^{T} \Delta C_p dT\right) - T\left(\Delta S_{298}^0 + \int_{298}^{T} \frac{\Delta C_p}{T}dT\right)\right.$$

$$\left. + RT \ln Q\right] \qquad [10]$$

where ΔG_T is the change in Gibbs free energy at a temperature T and 1 atm, ΔG_T^0, ΔH_T^0, and ΔS_T^0 are the changes in Gibbs free energy, enthalpy, and entropy that accompanies the formation of 1 mole of a product from its component elements at a temperature T and 1 atm, respectively, ΔC_P is the change in specific heat at constant pressure (1 atm), n is the number of electrons transferred in the half-cell reaction, F is the Faraday constant, R is the gas constant, T is the absolute temperature in kelvins, and Q is the reaction quotient.[24-27] Table II shows calculated results of the oxidation–reduction potentials of all the partial reactions considered. Activity of each chemical in the reaction quotient is substituted by the same value as the actual molar concentration of the chemical in the present reaction system, and specifically, both activities of H$_2$ and NH$_3$, which cannot be determined exactly, are substituted by 10^{-6} to obtain referential values. As shown in Table II, all the oxidation–reduction potentials shift to the negative direction with increasing both pH and temperature, which can result in a negative shift of the mixed potential. Even the oxidation–reduction potentials of Reactions 3 and 4 shift to the negative direction with increasing pH; the former is normally constant with pH and the latter increases with the increase in pH at a constant activity of Cu(II) ions. This is because, for example, the equilibrium activity of Cu^{2+} aquo ion decreases with increasing pH under the coexistence of abundant solid CuO in equilibrium, which brings about the negative shift of the oxidation–reduction potentials of Reactions 3 and 4. Thus, possibly the mixed potential is shifted to the negative direction with increasing pH and temperature because the oxidation–reduction potentials of all the partial reactions shift to the negative direction. Consequently, factors to change the mixed potential are pH and temperature, which are easily controllable.

Experimental

Procedure.— Reaction solutions were prepared using cupric oxide (CuO) (Kanto Chemical, Inc.), sodium hydroxide (NaOH), hydrazine monohydrate (N$_2$H$_4$·H$_2$O) (Nacalai Tesque, Inc.), and gelatin (Jellice Co. Ltd., P459) as received. All chemicals except for
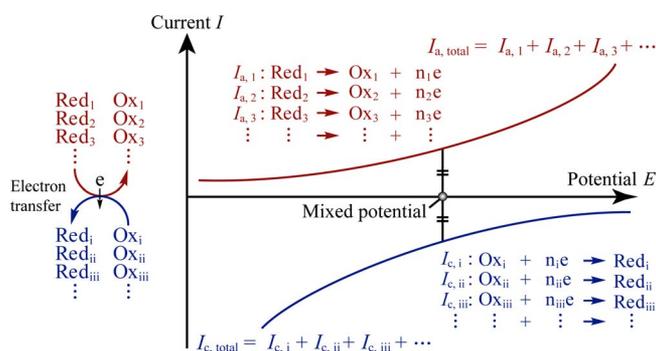

Figure 1. (Color online) Schematic potential–current curves: Mixed potential is determined at the value where the total of anodic currents $I_{a,total}$ balances the total of cathodic currents $I_{c,total}$ unless current flows outside.
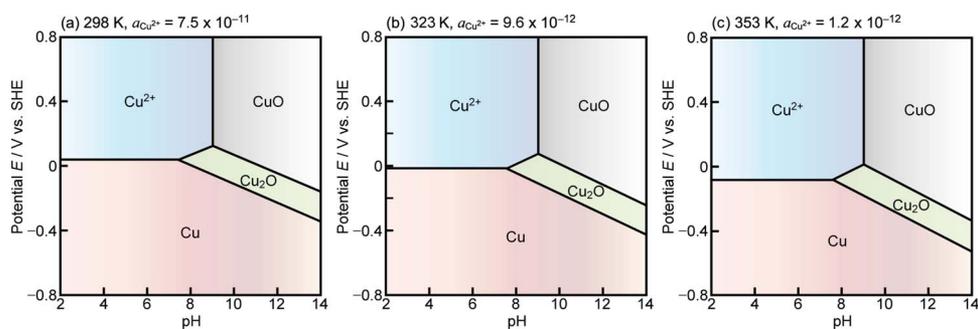
Figure 2. (Color online) Potential–pH diagrams drawn at the equilibrium activities of Cu^{2+} aquo ion at pH 9 and (a) 298, (b) 323, and (c) 353 K considering the species Cu^{2+}, CuO, Cu_2O, and Cu. Oxyanions of copper, $HCuO_2^-$ and CuO_2^{2-}, or hydroxyanions of copper, $Cu(OH)_3^-$ and $Cu(OH)_4^{2-}$, are not considered for simplicity. These potential–pH diagrams are only valid at the vertical line of pH 9 because the equilibrium activity of Cu^{2+} aquo ion changes with pH in this system.

gelatin were of reagent grade. Gelatin was added as a dispersing agent to avoid agglomeration and for the suppression of particle growth. Gelatin blocked oxygen and was also effective in preventing the oxidation of the resulted nanoparticles. Reactions were conducted in a Pyrex beaker 250 cm³ in capacity by the following procedure. First, a CuO colloidal aqueous suspension was prepared by dispersing 0.060 mole of CuO particles in 42.0 cm³ of distilled water using ultrasound. Next, 18.0 cm³ of 10 wt % gelatin aqueous solution was added into the solution as a dispersing agent. The initial pH of the mixed solution was adjusted to the reaction pH (9.0–12.0) at 298 K by 1.0 mol dm⁻³ sodium hydroxide aqueous solution with a pH meter (Horiba, Ltd., D-21). The temperature of the solution was kept at the reaction temperature (298–353 K) in a water bath with nitrogen gas bubbling (50 cm³ min⁻¹), which started 30 min before the reaction and lasted throughout the reaction to eliminate the effect of dissolved oxygen. The solution was agitated at a rate of 500 rpm with a magnetic stirring unit. Then, 42.0 cm³ of 1.43 mol dm⁻³ hydrazine aqueous solution was added to 18.0 cm³ of 10 wt % gelatin aqueous solution, and this solution was kept at the reaction temperature (298–353 K) with nitrogen gas bubbling (50 cm³ min⁻¹) for 30 min. The initial pH of the hydrazine solution was adjusted to the reaction pH (9.0–12.0) by 1.0 mol dm⁻³ sodium hydroxide aqueous solution at 298 K. Next, the hydrazine solution was added to the CuO aqueous suspension as a reducing agent to start the reaction. The total amount of the reaction suspension was 120.0 cm³, and thus the reaction suspension was 0.50 mol dm⁻³ hydrazine aqueous solution with 0.50 mol dm⁻³ dispersed CuO. Gelatin was not added in the reaction suspension at 298 K because gelatin became a gel at 298 K, inhibiting the reaction.

The crystalline structure of precipitates was investigated by X-ray diffraction (XRD: MAC Science Co., Ltd., M03XHF22) using a molybdenum X-ray tube. The morphology of precipitates was observed using a field-emission scanning electron microscope (JEOL Ltd., JSM-6500F). The immersion potential of Au-sputtered round quartz-crystal substrates 5.0 mm diameter was measured during several experimental runs by a potentiostat/galvanostat (Hokuto Denko Co., Ltd., HA-151), and the authors assumed that the measured immersion potential was almost the same as the mixed potential in reaction suspension in this system. A Ag/AgCl electrode (Horiba, Ltd., 2565A-10T) was used as a reference electrode, and the internal liquid, 3.33 mol dm⁻³ KCl aqueous solution, was replaced for each experimental run. The measured potential was converted to values vs standard hydrogen electrode (SHE) using the following empirical equation given by Horiba, Ltd.: The potential of the reference electrode could be expressed as a function of temperature T (K) as E (mV) vs SHE = +206 − 0.7(T − 298).

Results and Discussion

In the present method, pH of the reaction suspension is initially adjusted at 298 K, and actual pH at reaction temperatures differs from the adjusted value. This is ascribable to the change in the ionic product for water, $K_w = [H^+][OH^-]$; for example, the value of K_w (mol² dm⁻⁶) is 1.008×10^{-14} at 298.15 K and 5.476×10^{-14} at 323.15 K. Figure 3 shows the change with temperature in pH, which is initially adjusted to 9.0 at 298 K. pH linearly decreases with increasing temperature, and the values are 9.0 at 298 K, 8.5 at 323 K, and 7.6 at 353 K. Figure 4 shows the change in the mixed potential during the reaction for 2 h. At the same temperature of 323 K, the mixed potential at pH 10.4 (Fig. 4d) is lower than that at pH 8.5 (Fig. 4b). This agrees well with the discussion in the Theory section. Moreover, the mixed potential shifts to the negative direction with increasing temperature although pH slightly decreases, indicating that the mixed potential can be lowered just by increasing temperature without fixing pH.

By comparing the mixed potential and the potential–pH diagrams shown in Fig. 5, the mixed potential was in the stability region of Cu_2O both at pH 9.0, 298 K (Fig. 5a) and pH 8.5, 323 K (Fig. 5b), whereas the mixed potential was in the stability region of metal Cu at pH 7.6, 353 K (Fig. 5c). Figure 6 shows the change with time in XRD patterns of precipitates during the reaction for 2 h. CuO powder was reduced to Cu_2O after 1 h at pH 9.0, 298 K although slight Cu peaks are recognized in the XRD pattern taken at 2 h. At pH 7.6, 353 K, CuO powder was completely reduced to metal Cu after 0.5 h. These results are almost consistent with the result that the

Table II. List of oxidation–reduction potentials calculated for partial reactions considered in this system. Activity of each chemical species is substituted by the actual molar concentration in the present reaction system, and specifically, activities of H_2 and NH_3 are both substituted by 10^{-6} to obtain reference values. All the oxidation–reduction potentials calculated shift to the negative direction with increasing both pH and temperature, which can result in a negative shift of the mixed potential.

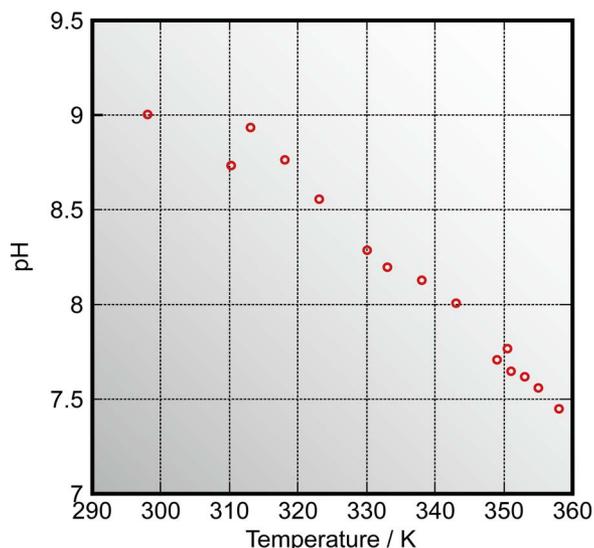| Partial reaction	Oxidation–reduction potential at pH 9 (V vs SHE)			Oxidation–reduction potential at pH 12 (V vs SHE)			Reaction no.
	298 K	323 K	353 K	298 K	323 K	353 K	
$N_2 + 4H_2O + 4e = N_2H_4 + 4OH^-$	−0.92	−0.98	−1.06	−1.09	−1.17	−1.27	1
$\frac{1}{2}N_2 + NH_3 + H_2O + e = N_2H_4 + OH^-$	−2.59	−2.72	−2.88	−2.777	−2.91	−3.09	2
$Cu(II) + 2e = Cu$	0.04	−0.02	−0.08	−0.14	−0.21	−0.29	3
$2Cu(II) + 2OH^- + 2e = Cu_2O + H_2O$	0.13	0.07	0.01	−0.05	−0.12	−0.20	4
$2H_2O + 2e = H_2 + 2OH^-$	−0.18	−0.19	−0.21	−0.35	−0.38	−0.42	5

Figure 3. (Color online) Change in pH of the reaction suspension with temperature; pH of the reaction suspension was initially adjusted to 9.0 at 298 K.
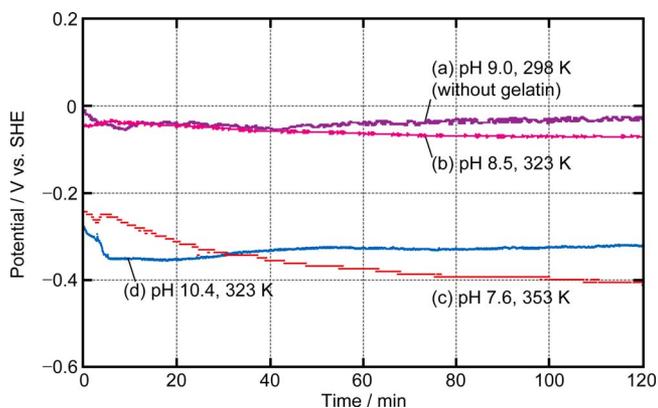

Figure 4. (Color online) Mixed potentials measured during the reaction at (a) pH 9.0, 298 K (without gelatin), (b) pH 8.5, 323 K, (c) pH 7.6, 353 K, and (d) pH 10.4, 323 K.
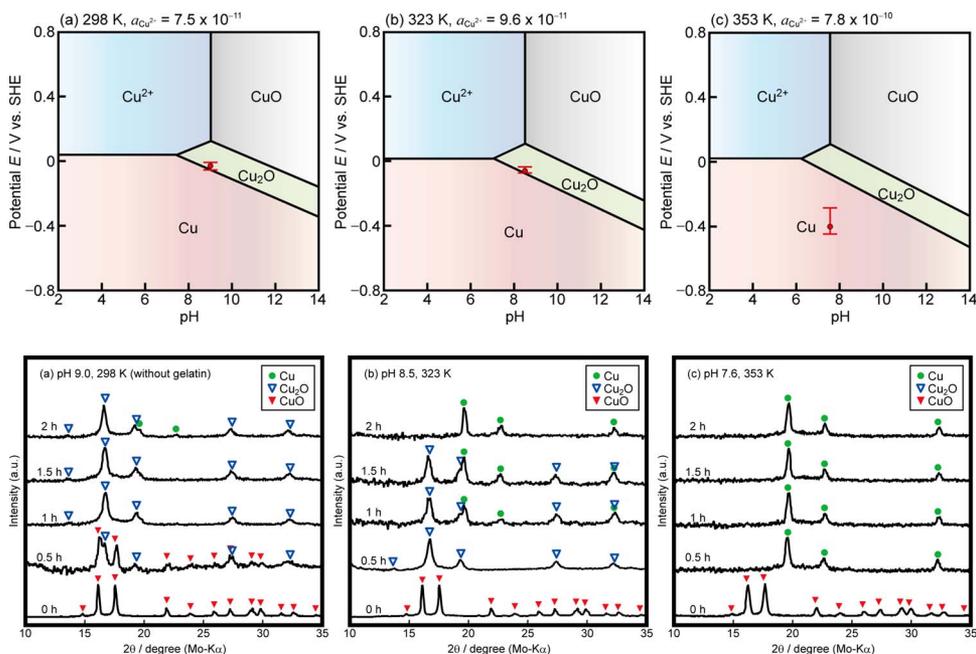
mixed potentials measured at pH 7.6, 353 K and pH 9.0, 298 K were always in the stability region of Cu and Cu_2O, respectively. In contrast, at pH 8.5, 323 K, all CuO powder was reduced to Cu_2O after 0.5 h and then the resulting Cu_2O was gradually reduced to Cu metal. This is not consistent with the measurement result of the mixed potential. By carefully observing the change in the mixed potential at pH 8.5, 323 K, the initial mixed potential is -0.045 V vs SHE and in the stability region of Cu_2O, and the mixed potential gradually decreases to -0.072 V with reaction time, which is just beside the calculated oxidation–reduction potential of Cu_2O/Cu, -0.077 V vs SHE; i.e., as CuO is reduced to Cu_2O, the mixed potential approaches the oxidation–reduction potential of Cu_2O/Cu redox pair, where Cu_2O and Cu coexist. Nevertheless, the mixed potential is 5 mV higher than the calculated oxidation–reduction potential of Cu_2O/Cu and it is difficult to adequately elaborate on the result that the deposition of Cu completely proceeded after 2 h. Here, pH of the solution tends to slightly decrease during the reaction, although ideally, pH would not be changed by taking into account the overall reaction in the present reaction system. For example, pH actually decreased from 8.5 to approximately 8 at 323 K, resulting in a slight increase in the oxidation–reduction potential of a Cu_2O/Cu redox pair. Furthermore, there can be a slight difference between the mixed potential measured using Au electrode and the actual mixed potential in the reaction suspension. Therefore, the actual mixed potential is slightly lower than the oxidation–reduction potential of the Cu_2O/Cu redox pair. Nonetheless, a Au electrode is preferable for the measurement of the mixed potential in this reaction system because a Au electrode does not have intense catalytic activity for a specific partial reaction possible in the reaction system,[30,31] and the effect of the immersion of the Au substrate is extremely low.

The scanning electron microscopy (SEM) images of the precipitates obtained by the reaction are shown in Fig. 7. Relatively large Cu_2O particles with an average diameter of 475 nm are observed in the precipitates obtained after 2 h at pH 9.0, 298 K. These large particles are attributable to the absence of gelatin. At pH 8.5, 323 K, Cu_2O particles with an average diameter of 97 nm are observed after 0.5 h and Cu particles with an average diameter of 82 nm are observed after 2 h. Cu particles with an average diameter of 55 nm are observed after 2 h at 353 K. As above, the mean particle size is decreased with the increase in temperature because nucleation site increases with the increase in temperature and an inordinate number
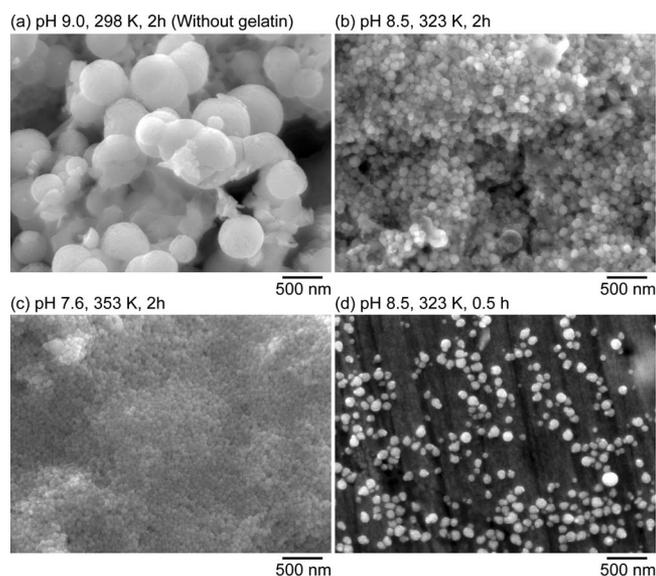

Figure 5. (Color online) Potential–pH diagrams drawn at the equilibrium activities of Cu^{2+} aquo ion at (a) pH 9.0, 298 K, (b) pH 8.5, 323 K, and (c) pH 7.6, 353 K considering the species Cu^{2+}, CuO, Cu_2O, and Cu. Bars and circles indicate the range and average value of the measured mixed potential, respectively.

Figure 6. (Color online) XRD patterns of precipitates obtained during the reaction at (a) pH 9.0, 298 K (without gelatin), (b) pH 8.5, 323 K, and (c) pH 7.6, 353 K for 2 h.

Figure 7. SEM images of precipitates obtained by the reaction at (a) pH 9.0, 298 K (without gelatin), (b) pH 8.5, 323 K, (c) pH 7.6, 353 K for 2 h, and (d) pH 8.5, 323 K for 0.5 h.

of nucleation sites at high temperatures leads to the absence of reactant ions [Cu(II) or Cu(I) ions] for the growth. Table III shows the crystallite sizes of particles obtained by chemical reduction, which were calculated by Scherrer's equation using the peak width at half-maximum of 111 peaks at $2\theta = 16.5°$ for Cu_2O and $19.6°$ for Cu. The crystallite sizes are all much smaller than those of particles observed, and possibly these particles are all polycrystalline. This result indicates that the deposition rate of Cu and Cu_2O nanoparticles is significantly large for the formation of single-crystal nanoparticles in the present method. The large reaction rate is industrially favorable. Single-crystal Cu and Cu_2O nanoparticles can be obtained by regulating the deposition of nanoparticles using a milder reducing agent than hydrazine or adding a strong complexing agent.

Conclusions

A general concept for oxidation-state control of nanoparticles synthesized via chemical reduction has been developed. Through the present work, we have obtained the following results.

Mixed potential is the most effective indicator of solution circumstances, indicating the most stable chemical species in the reaction solution, i.e., thermodynamic considerations in conjunction with monitoring of mixed potential is useful for the in situ predic-

tion of "what chemical species will be synthesized." Solution pH and temperature are the factors which affect the mixed potential, and thus, the most stable chemical species can be changed by pH and temperature. Specifically in this system, the mixed potential decreases with the increase both in pH and temperature. Using this concept, we demonstrated the selective synthesis of Cu and Cu_2O nanoparticles by controlling mixed potential. This concept is also effective in other reaction systems where thermodynamic data are available.

References

1. W. K. Han, K. W. Choi, G. H. Hwang, S. J. Hong, J. S. Lee, and S. G. Kang, *Appl. Surf. Sci.*, **252**, 2832 (2006).
2. L. Huang, H. Jiang, J. Zhang, Z. Zhang, and P. Zhang, *Electrochem. Commun.*, **8**, 262 (2006).
3. L. Yu, H. Sun, J. He, D. Wang, X. Jin, X. Hu, and G. Z. Chen, *Electrochem. Commun.*, **9**, 1374 (2007).
4. I. Lisiecki and M. P. Pileni, *J. Am. Chem. Soc.*, **115**, 3887 (1993).
5. I. Lisiecki, F. Billoudet, and M. P. Pileni, *J. Phys. Chem.*, **100**, 4160 (1996).
6. H. H. Huang, F. Q. Yan, Y. M. Kek, C. H. Chew, G. Q. Xu, W. Ji, P. S. Oh, and S. H. Tang, *Langmuir*, **13**, 172 (1997).
7. L. Qi, J. Ma, and J. Shen, *J. Colloid Interface Sci.*, **186**, 498 (1997).
8. H. Ohde, F. Hunt, and C. M. Wai, *Chem. Mater.*, **13**, 4130 (2001).
9. N. A. Dhas, C. P. Raj, and A. Gedanken, *Chem. Mater.*, **10**, 1446 (1998).
10. R. V. Kumar, Y. Mastai, Y. Diamant, and A. Gedanken, *J. Mater. Chem.*, **11**, 1209 (2001).
11. M.-S. Yeh, Y.-S. Yang, Y.-P. Lee, H.-F. Lee, Y.-H. Yeh, and C.-S. Yeh, *J. Phys. Chem. B*, **103**, 6851 (1999).
12. S. S. Joshi, S. F. Patil, V. Iyer, and S. Mahumuni, *Nanostruct. Mater.*, **10**, 1135 (1998).
13. A. P. Young and C. M. Schwartz, *J. Phys. Chem. Solids*, **30**, 249 (1969).
14. J. Zhang, J. Liu, Q. Peng, X. Wang, and Y. Li, *Chem. Mater.*, **18**, 867 (2006).
15. D. Snoke, *Science*, **298**, 1368 (2002).
16. A. Muramatsu and T. Sugimoto, *J. Colloid Interface Sci.*, **189**, 167 (1997).
17. X. Liu, B. Geng, Q. Du, J. Ma, and X. Liu, *Mater. Sci. Eng., A*, **448**, 7 (2007).
18. L. Gou and C. J. Murphy, *Nano Lett.*, **3**, 231 (2003).
19. R. Liu, F. Oba, E. W. Bohannan, F. Ernst, and J. A. Switzer, *Chem. Mater.*, **15**, 4882 (2003).
20. C. Lu, L. Qi, J. Yang, X. Wang, D. Zhang, J. Xie, and J. Ma, *Adv. Mater. (Weinheim, Ger.)*, **17**, 2562 (2005).
21. W. Wang, G. Wang, X. Wang, Y. Zhan, Y. Liu, and C. Zheng, *Adv. Mater. (Weinheim, Ger.)*, **14**, 67 (2002).
22. S. Yagi, H. Nakanishi, E. Matsubara, S. Matsubara, T. Ichitsubo, K. Hosoya, and Y. Matsuba, *J. Electrochem. Soc.*, **155**, D474 (2008).
23. S. Yagi, T. Koyanagi, H. Nakanishi, T. Ichitsubo, and E. Matsubara, *J. Electrochem. Soc.*, **155**, D583 (2008).
24. C. M. Criss and J. W. Cobble, *J. Am. Chem. Soc.*, **86**, 5385 (1964).
25. W. M. Latimer, *The Oxidation States of the Elements and Their Potentials in Aqueous Solutions*, 2nd ed., Prentice-Hall, Englewood Cliffs, NJ (1959).
26. O. Kubaschewski and C. B. Alcock, *Metallurgical Thermochemistry*, 5th ed. revised and enlarged, Elsevier, New York (1979).
27. D. R. Stull and H. Prophet, *JANAF Thermochemical Tables*, 2nd ed., NSRDS-NBS, Washington, DC (1971).
28. M. Pourbaix, *Atlas of Electrochemical Equilibria in Aqueous Solutions*, p. 384, Cebelcor, Brüssel (1966).
29. B. Beverskog and I. Puigdomenech, *J. Electrochem. Soc.*, **144**, 3476 (1997).
30. C. D. Iacovangelo, *J. Electrochem. Soc.*, **138**, 976 (1991).
31. C. D. Iacovangelo and K. P. Zarnoch, *J. Electrochem. Soc.*, **138**, 983 (1991).

Table III. Crystallite sizes of particles obtained by chemical reduction. Calculation was conducted using Scherrer's equation with the half-width of 111 peak.

	Half-width (deg)	Diffraction angle 2θ (deg)	Crystallite size (nm)
pH 9.0, 298 K, 2 h (Cu_2O)	0.359	16.5	10.3
pH 8.5, 323 K, 2 h (Cu)	0.209	19.6	17.8
pH 7.6, 353 K, 2 h (Cu)	0.252	19.6	14.8
pH 8.5, 323 K, 0.5 h (Cu_2O)	0.431	16.5	8.6